Spectral Evolution of Galaxies

Stéphane Charlot [1,2]

[1]Institut d'Astrophysique du CNRS, 98 bis Boulevard Arago, F-75014 Paris, France
[2]Kitt Peak National Observatory, 950 N. Cherry Avenue, Tucson, AZ 85726, U.S.A.

Abstract: We review models of spectral evolution of galaxies and current constraints set by observations at high redshifts on the formation and evolution of galaxies. These lectures assume previous basic knowledge of the general properties of stars and galaxies.

1 Stellar Population Synthesis

1.1 Introduction

The integrated light from star clusters and galaxies should reflect the distribution of stellar masses, ages, and metallicities within them, providing us with important clues on the past history of star formation. Stellar population synthesis, the modeling of the spectral energy distribution emitted by specific populations of stars, is a natural approach to identifying such clues. Studies in this field have led to the development of population synthesis models, usually termed "evolutionary" (Crampin & Hoyle 1961; Tinsley 1978; Bruzual 1983; Arimoto & Yoshii 1987; Guiderdoni & Rocca-Volmerange 1987; Buzzoni 1989; Bruzual & Charlot 1993, 1996; Bressan, Chiosi, & Fagotto 1994; Fritze von Alvensleben & Gehrard 1994; Worthey 1994; Mayya 1995; Weiss, Peletier, & Matteucci 1995). In such models the detailed physical processes affecting gas properties and star formation efficiency in a galaxy are generally all reduced to few crude assumptions about the stellar birthrate (the relative efficiency of the various processes involved are extremely difficult to determine, even in nearby star-forming regions; e.g., Silk 1996). The main adjustable parameters are then usually the stellar initial mass function (IMF), the star formation rate, and in some cases the rate of chemical enrichment. For a given set of these parameters one computes the time-dependent distribution of stars in the theoretical Hertzsprung-Russell diagram (hereafter H-R diagram), from which the integrated spectral evolution of the stellar population can be obtained. These models are widely used to study

stellar systems which are too far away for individual stars to be discerned. In particular, they constitute an essential tool of observational cosmology.

We first briefly mention the basic ingredients and simplifying assumptions underlying population synthesis models (see, e.g., Tinsley 1980 for more details). The IMF, noted $\phi(m)$, is defined in such a way that $\phi(m)dm$ is the number of stars born with masses between m and $m + dm$. We use here the normalization

$$\int_{m_L}^{m_U} dm\, m\phi(m) = 1\, M_\odot. \tag{1}$$

The lower and upper mass cutoffs are still subject to debate (e.g., Scalo 1986, and references therein). Standard values are $m_L = 0.1\, M_\odot$ and $m_U = 100\, M_\odot$. Salpeter (1955) has shown from star counts that the IMF in the solar neighborhood is well represented by a single power law

$$\phi(m) = m^{-(1+x)}, \tag{2}$$

with a slope $x = 1.35$. More recent studies suggest that the IMF probably has a flatter slope at lower masses, and that it might even be bimodal, with low-mass and high-mass stars forming in different environments and at different rates (e.g., Larson 1986; Scalo 1986; see Silk 1996 for a review of current theories of star formation).

In general, in population synthesis models the IMF is assumed to be constant in time, space, and metallicity and to be similar to that in the solar neighborhood. The other main free parameters, the star formation and chemical enrichment rates, are then to be constrained by observations. The star formation rate is defined as the mass of gas transformed into stars per unit time,

$$\psi(t) = -dM_g/dt. \tag{3}$$

Stars form heavy elements and return enriched matter into the interstellar medium, especially at the end of their lives. Hence, chemical enrichment is a natural product of stellar evolution in galaxies. The chemical enrichment rate is defined as the increase per unit time in the mass fraction Z of all elements heavier than helium in the gas phase,

$$\chi(t) = dZ/dt. \tag{4}$$

The parameter Z is usually called "metallicity" of the gas, and its value in the solar neighborhood is $Z \approx 0.02$ (the mass fractions of hydrogen and helium are $X \approx 0.70$ and $Y \approx 0.28$, respectively; hence $X+Y+Z = 1$). A full understanding of galaxy evolution therefore requires that chemical and spectral evolution be treated consistently. However, the connection between ψ and χ is not trivial, as it is likely to depend on location, age, and environment. Hence, it appears more tractable at first, if not necessary, to study separately models of chemical and spectral evolution of galaxies. By combining the two types of models, one can hope to eventually arrive at a rough understanding of galaxy evolution.

Spectral evolution of galaxies can be investigated without prior knowledge of chemical evolution because galaxies with any star formation histories can

be expanded in series of instantaneous bursts, each having fixed metallicity. Thus, the spectral energy distribution $F_\lambda(t)$ at age t of a stellar population with arbitrary star formation rate and chemical enrichment rate can be modeled by means of a simple convolution integral of the spectra $F_Z(t')$ of instantaneous-burst populations with age t' and metallicity $Z(t-t')$ as,

$$F_\lambda(t) = \int_0^t d\tau \psi(t-\tau) F_{Z(t-\tau)}(\tau). \tag{5}$$

The first goal of population synthesis models is therefore to build accurate spectral evolution models $F_Z(t)$ for instantaneous-burst stellar population with fixed Z, the influence of chemical enrichment in the determination of $Z(t)$ appearing only as the next order complication. This generalized approach to the spectral evolution of galaxies is known as "isochrone synthesis" (Charlot and Bruzual 1991; see §1.2 below). It also implies that the properties predicted for any stellar population can be traced back to those of isochrones predicted for instantaneous burst populations with fixed metallicities. In §1.2 below, we describe the general principles of stellar population synthesis models and review standard results about the spectral evolution of galaxies with different star formation histories. Then, in §1.3, we investigate the main uncertainties underlying the predictions of current population synthesis models and prospects for future improvement.

1.2 Concepts of Spectral Evolution

In this section we describe the various steps involved in the modeling of spectral evolution of galaxies and present the most significant results usually inferred from population synthesis models. To perform isochrone synthesis we must first compute accurate isochrones in the theoretical H-R diagram for instantaneous-burst stellar population with fixed metallicities and in a wide range of ages. An isochrone at age t is defined by the loci in the H-R diagram of stars born coevally at $t = 0$ with masses distributed according to the IMF. This can be computed from the predictions of stellar evolution theory for the evolutionary tracks followed in the H-R diagram by individual stars with given initial mass and metallicity.

We recall that stars can generally be arranged into three main mass ranges, within which the various stages of evolution are similar. *Massive* stars ($m \gtrsim 8\ M_\odot$) go through all nuclear burning phases until the formation of an iron core. Their subsequent fate is either a type II or Ib supernova, followed by the formation of a neutron star or a black hole. *Intermediate-mass* stars have initial masses in the range $M_{\rm HeF} \lesssim m \lesssim M_{\rm up}$. Here, $M_{\rm HeF} \approx 1.9\ M_\odot$ is the minimum mass limit for quiet He-ignition while $M_{\rm up} \approx 5 - 7 M_\odot$ is roughly the maximum mass limit for degenerate C-ignition (the values of these characteristic masses are somewhat model dependent). After core-He exhaustion, intermediate-mass stars ignite helium in a shell which expands outward, and causes the surrounding hydrogen shell to extinguish. This constitutes the early AGB phase, since stars then undertake their second ascent of the giant branch in the H-R diagram.

Although the detail of the evolution along the AGB depends on initial mass, all stars re-ignite their hydrogen shell at some point and enter a double-shell burning phase characterized by the periodic thermal pulses of the He-shell. This constitutes the thermally pulsing AGB phase. Intermediate-mass stars then lose their envelope, leading to the formation of a planetary nebula nucleus (PNN) that evolves into a white dwarf (WD). The evolution of stars with masses in the range $5-7 \lesssim m \lesssim 8\ M_\odot$ is uncertain. They most likely undergo non-degenerate (off-center) C-ignition at the end of their early AGB evolution, and they could either become WDs if they lose enough mass or collapse as neutron stars. Finally, *low-mass* stars ($0.08 M_\odot \lesssim M_{\rm HeF}$) ignite helium degenerately (the "He-Flash") at the tip of the red giant branch (RGB), afterwhich their evolution is similar to that of intermediate-mass stars.

Figure 1 illustrates the evolutionary tracks followed in the theoretical H-R diagram by stars in the main mass ranges described above. The tracks are from the solar metallicity computations of Bressan et al. (1993). The evolutionary lifetime along the tracks, 90% of which is spent burning hydrogen on the main sequence, is a strong decreasing function of initial mass, roughly $t_{\rm evo} \approx 10^{10}(m/M_\odot)^{-2}$ yr.

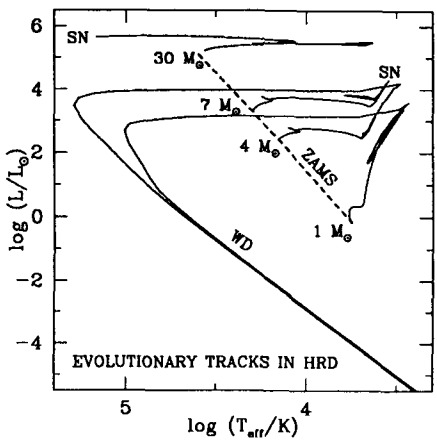

Fig. 1. Evolutionary tracks of stars with solar metallicity in the theoretical H-R diagram (from Bressan et al. 1993). The tracks start on the zero-age main sequence (ZAMS). Low- and intermediate-mass stars terminate their evolution as white dwarfs (WD) and massive stars as supernovae (SN).

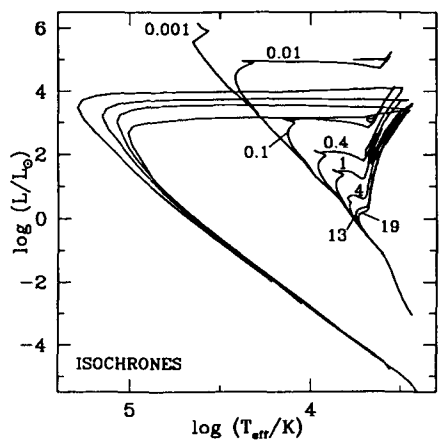

Fig. 2. Theoretical isochrones interpolated at various ages, as described in the text, from a complete set of evolutionary tracks of stars with solar metallicity and initial masses in the range $0.1 \leq m \leq 100\ M_\odot$. Ages are indicated in Gyr next to the isochrones.

We note that the "turnoff" effective temperature and luminosity of a star roughly scale with initial mass as $T_{\rm eff} \propto m^{0.5}$ and $L \propto m^3$ (a characteristic turnoff marks the end of core-H burning in the H-R diagram when the star leaves the main sequence and starts to cool; both scaling relations flatten at large m). To construct accurate isochrones at various ages for an instantaneous burst stellar population,

one must first identify stages of equivalent physical significance (e.g., the end of core-H burning) among a sample of evolutionary tracks for a complete set of initial masses, some stages being defined only in a restricted mass range (e.g., the He-flash for low-mass stars). An isochrone that corresponds to a continuous distribution of initial masses is then defined by interpolation from the evolutionary tracks at a fixed age t of the loci in the H-R diagram of stars in all evolutionary stages. Figure 2 shows examples of isochrones computed using a full set of 28 evolutionary tracks for solar-metallicity stars from Bressan et al. A total of 310 evolutionary phases were identified to define the isochrones. The number of stars in each evolutionary phase along the isochrones is given by the IMF weight, $\phi(m)$, and the (interpolated) time spent in that phase.

The integrated spectral energy distribution of the stellar population at a given age is simply the sum of the spectra of stars along the isochrone at that age. Before we proceed with a detailed modeling, it is worth noting that the behavior of the integrated optical spectrum of a stellar population can be guessed from a simple reasoning neglecting the contribution from advanced stages of stellar evolution (evolved stars contribute mainly at infrared wavelengths; see below). We first remark that the spectrum of a star can be roughly approximated by that of a blackbody of same temperature and luminosity related by the Stefan-Boltzmann law, $L = 4\pi R^2 \sigma T_{\rm eff}^4$.[1] Therefore, the wavelength of maximum intensity of a stellar spectrum is, according to Wien's law, around $\lambda_{\rm max} = 2.9\,(T_{\rm eff}/1000{\rm K})^{-1}\,\mu$m (if intensity is defined per unit wavelength). Since massive stars have larger luminosities and higher temperatures than low-mass stars, their spectra are brighter and peak at shorter wavelengths. Photometrically, this implies that massive stars are bluer than low-mass stars (see eq. [6] below). Thus, if stars of all masses are assumed to be born at once and with an IMF similar to that in the solar-neighborhood (eq. [1]), the fractional contribution to the integrated spectrum by stars of mass m will scale initially as $L(m)\phi(m) \propto m^{0.65}$. We then expect blue, short-lived massive stars to strongly dominate the optical spectrum at early ages. After these stars disappear, the optical spectrum must fade rapidly and redden as less massive, cooler stars dominate the light.

We now investigate in more detail the spectral evolution of an instantaneous burst stellar population. To begin with, we show in Figure 3 how the actual spectrum of a star (a solar-metallicity, main-sequence star with $\log T_{\rm eff} = 3.6$) compares with that of a pure blackbody of same temperature. Although the two spectra have similar shapes, line blanketing by many atomic transitions in the stellar atmosphere reduces substantially the emerging radiation with respect to a pure blackbody model. Therefore, stellar spectra cannot be reliably approximated by unblanketed blackbody spectra, and one of the main difficulties in

[1] The present argument is useful mostly to provide a schematic idea of the optical spectral properties of a stellar population. In reality, the radius entering the Stefan-Bolztmann relation is not well defined for evolved (post-main sequence) stars with extended thick envelopes, in which radiation emerges from different radii at different wavelengths. In such cases, $T_{\rm eff}$ can be considerably larger than the actual radiation temperature at most wavelengths.

building a population synthesis is to assemble a complete library of individual spectra for stars in wide ranges of temperature, luminosity, and metallicity.

Figure 4 shows the spectral evolution of an instantaneous burst stellar population with solar metallicity computed using such a complete library of stellar spectra and summing the spectra of individual stars along the isochrones shown in Figure 2 (from Bruzual & Charlot 1996). As expected, at 10^6 yr the spectrum is entirely dominated by short-lived, young massive stars on the main sequence and peaks in the ultraviolet. After 1×10^7 yr, the most massive stars have evolved off the main sequence and become red supergiants, making the ultraviolet light decline and the near-infrared light rise. From a few times 10^8 yr to $\gtrsim 1 \times 10^9$ yr, the AGB stars maintain a high near-infrared luminosity, and the ultraviolet light continues to drop as the turnoff mass decreases on the main sequence. After a few times 10^9 yr, the RGB takes over the production of the near-infrared light. The rise in the far ultraviolet after 4–10 Gyr is produced by low-mass stars in their post-AGB evolution. The most remarkable feature in Figure 4 is the nearly unevolving shape of the optical to near-infrared spectrum at ages from 4 to 19 Gyr. The reason for this is that low-mass stars evolve from the main sequence to the end of the AGB in a small range of temperatures (see Fig. 2).

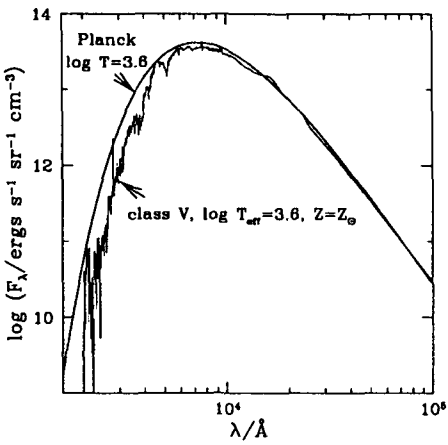

Fig. 3. Spectral energy distribution of a main sequence (luminosity class V) star with $\log T_{\rm eff} = 3.6$ compared to that of an unblanketed blackbody model with the same temperature.

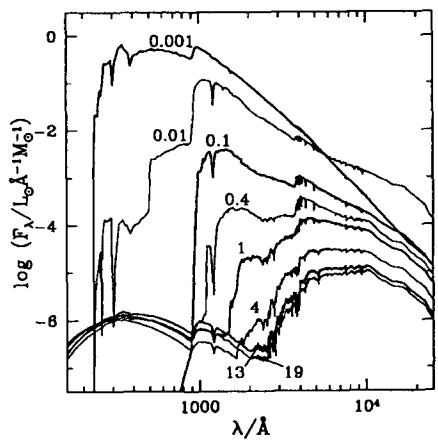

Fig. 4. Spectral evolution of an instantaneous burst stellar population with solar metallicity and a Salpeter IMF. Ages (in Gyr) are indicated next to the spectra.

For galaxies about which detailed spectral information is not available, colors indicating the flux emitted in broad spectral bands represent a useful alternative. Several systems can be chosen to define colors from a spectral energy distribution. In the standard color system, an $M_i - M_j$ "color index" (or simply "color") between two spectral bands M_i and M_j centered around two wavelengths $\lambda_i < \lambda_j$ is defined by

$$M_i - M_j = \text{zeropoint} - 2.5 \log(F_i/F_j), \qquad (6)$$

where $F_k = \int d\lambda R_{k,\lambda} F_\lambda$ (in units of erg s^{-1} cm^{-2}) is the convolution of the spectrum F_λ by the response function $R_{k\lambda}$ of the $k^{\rm th}$ filter. Hence, by definition, a color is bluer when it is more negative. The zeropoint is defined in such a way that for the standard A0V star Vega, $M_i - M_j$ is always zero and the V magnitude is 0.03 (see Thuan & Gunn 1976; and Oke & Gunn 1983 for definitions of other photometric and spectrophotometric systems). For reference, the effective wavelengths (and bandwidths) of the standard U, B, V, R, I, J, K, and L filters are, in μm, 0.359 (0.065), 0.441 (0.104), 0.547 (0.118), 0.652 (0.087), 0.827 (0.211), 1.33 (0.285), 1.71 (0.280), 2.15 (0.394), and 3.50 (0.540) respectively. As an application, Figure 5 shows the evolution of the $U-B$ and $V-K$ colors and mass-to-visual light ratio, M/L_V, for the instantaneous burst stellar population of Figure 4. As expected, the colors are bluest at early ages and redden progressively as the most massive stars terminate their evolution. However, after only a few billion years, the evolution is very slow. The mass-to-light ratio increases steadily with time because while the total mass of the stellar population remains constant, the V-band luminosity decreases together with the turnoff mass.

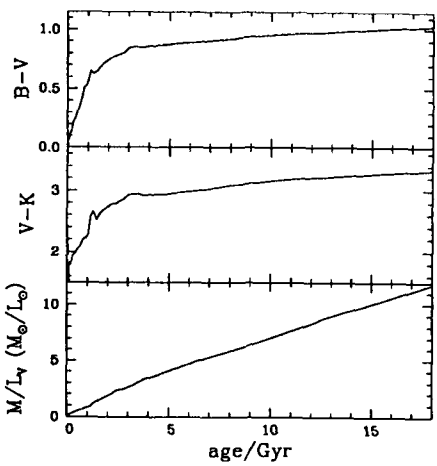

Fig. 5. Evolution of the $B-V$ and $V-K$ colors and mass-to-visual light ratio M/L_V for an instantaneous burst stellar population with solar metallicity and a Salpeter IMF.

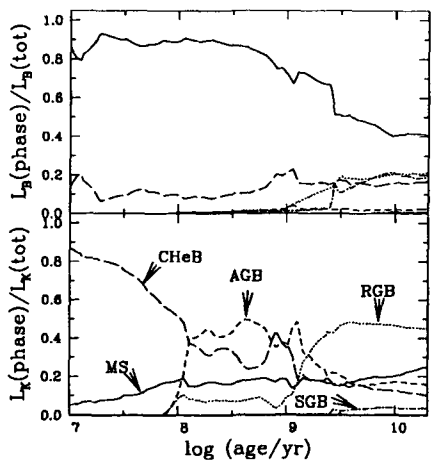

Fig. 6. Fractional contributions to the B and K light of the stellar population in Fig. 5 by stars on the main sequence and various post-main sequence evolutionary phases (see text for acronyms).

As an instructive complement to Figure 5, Figure 6 illustrates separately the evolution (here as a function of log age) of the contributions to the integrated B and K light by stars on the main sequence (MS) and in various post-main sequence evolutionary stages: subgiant branch (SGB; for low-mass stars), RGB, core-He burning phase (CHeB; which includes the supergiant phase for massive stars), and AGB. Main-sequence stars (essentially near the turnoff) dominate the integrated B light all ages. This justifies a posteriori the arguments used previously to describe spectral evolution in the optical from rough scaling re-

lations. In the K band, however, main sequence stars never account for more than 20% of the integrated light. The emission is dominated first by supergiants, and then by AGB descendants of intermediate-mass stars from about 1×10^8 to 1×10^9 yr. At later ages, the RGB progeny of low-mass stars accounts for nearly half the integrated infrared light.

The photometric evolution of galaxies with continuous star formation rates can be readily understood from equation (5) and the photometric evolution of an instantaneous burst stellar population in Figure 4. We fix for the moment the metallicity to the solar value and compute the spectral evolution of stellar populations with exponentially declining star formation rates $\psi(t) = \exp(-t/\tau)/\tau$, with timescales of star formation τ = 1, 2, 4, 7 Gyr, and ∞ (corresponding to $\psi(t)$ =constant). The results are shown in Figure 7, along with the mean observed colors of nearby galaxies of various morphological types (E to Irr).

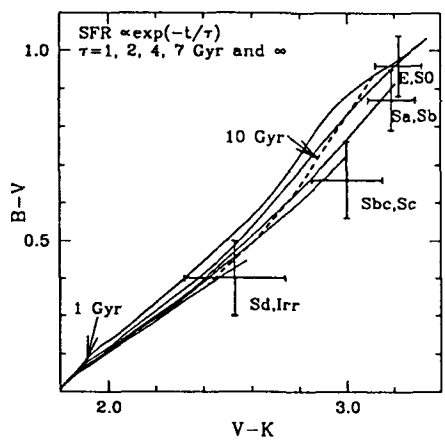

Fig. 7. Comparison of the $V - K$ and $B - V$ colors of models with various exponentially declining star formation rates with the observed colors of nearby galaxies of different morphological types. Timescales of star formation (in Gyr) are indicated next to the curves. Dashed lines show the location of the models at 1 and 10 Gyr.

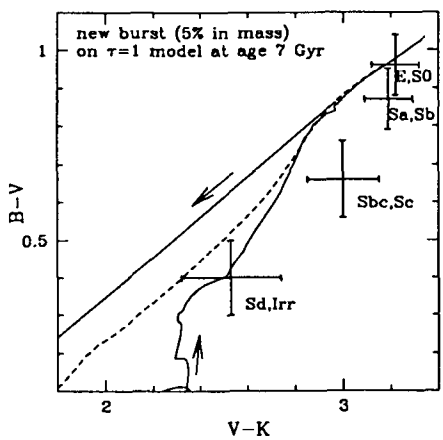

Fig. 8. The dashed line corresponds to the model with $\tau = 1$ Gyr in Fig. 7. The solid line shows the effect of adding a new burst of duration 10^8 yr on this model at an age of 7 Gyr, in which 5% of the final galaxy mass in stars is formed. Arrows indicate the sense of the rapid blueing and subsequent reddening that follow burst.

The models start in the blue region of the BVK plane (lower left) and evolve redward. The two dashed lines join the locations of the various models at fixed ages of 1 and 10 Gyr. All models follow a similar path in the BVK plane until about $\lesssim 1$ Gyr. Then, models with longer timescales of star formation remain relatively blue, evolving slowly toward the colors of later-type Spirals, whereas rapidly star-forming models redden faster and lead to the colors of early-type E/S0 galaxies. In fact, ongoing star formation in models with large τ's can maintain blue colors for as long as the stellar population is replenished in massive

stars. The modest reddening undergone by these models, which is more pronounced in $V-K$ than in $B-V$, is caused mainly by the accumulation old, low-mass RGB stars. As soon as star formation drops significantly, at ages $t > \tau$, the most massive stars disappear and colors redden rapidly.

The strong dominance of young massive stars in any stellar population has important consequences for determining the history of star formation in galaxies from their observed spectral energy distribution. As an introduction to this issue, we show in Figure 8 the evolutionary path in the BVK plane of a model galaxy with a short star formation timescale, $\tau = 1$ Gyr, on which a new burst of duration 10^8 yr and involving 5% of the final galaxy mass is superimposed at an age of 7 Gyr. The new addition of massive stars blues instantaneously the colors. In fact, less than 1 Gyr after the burst, the model galaxy has colors typical of a nearby irregular galaxy. Then, when massive stars terminate their evolution, the colors of the model galaxy in Figure 8 redden rapidly again, and less than 3 Gyr after the burst the galaxy appears virtually identical to what it would in the absence of recent star formation.

Figures 7 and 8 together suggest that, even at fixed metallicity, colors are degenerate indicators of the the past history of star formation in galaxies. Within less than 0.1 mag in $B-V$ and $V-K$ colors, an irregular galaxy can be modeled by either a 10 Gyr old stellar population with constant star formation rate, or a younger stellar population with a declining star formation rate, or even by an old, passively evolving stellar population with a small amount of recent star formation. Furthermore, E/S0 galaxies appear to have colors essentially characteristic of any stellar population in which star formation has ceased for at least a few billion years. This degeneracy of the appearance of galaxies relative to the past history of star formation remains even when the whole spectrum from the optical to infrared is considered instead of simply broad-band colors (e.g., Bruzual & Charlot 1993). This leads us to one of the most important conclusions about spectral evolution: the spectral continuum shape of a galaxy depends essentially only on the ratio of the present to past-averaged star formation rates. This may be roughly estimated as

$$\frac{\psi(\text{present})}{\langle\psi\rangle} \approx \frac{\psi(\text{present}) \times \text{age}}{M_*}, \tag{7}$$

where M_* is the total mass in stars. Evidently, $\psi(\text{present})/\langle\psi\rangle$ does not provide us with any information on absolute ages nor on the details of the past history of star formation. It is remarkable to note, however, that this ratio correlates well with galaxy morphological type. The observed values range from 0 for E/S0 galaxies to 0.1 for Sa/Sab galaxies, 1 for Sbc/Sc galaxies, and up to a few for Sm/Im galaxies (Gallagher, Hunter, & Tutukov 1984; Kennicutt, Tamblyn, & Congdon 1994).

Another useful prediction of population synthesis models is mass-to-light ratio, as this can ultimately help us to estimate the mass of a distant galaxy from its observed luminosity. Since very low-mass stars on the lower main sequence are very faint, they can contribute significantly to the mass but not to the

integrated light of a whole stellar population. Therefore, the lower cutoff of the IMF is a key uncertain parameter in determinations of mass-to-light ratios. The upper cutoff is a less critical parameter if the slope of the IMF is similar to that in the solar neighborhood. The reason for this is that, near the cutoff ($m \gtrsim 50\,M_\odot$), the luminosity depends less strongly on main sequence mass ($L \propto m^2$ instead of m^3 at turnoff). Hence the integrated mass and luminosity both depend very weakly on m_U, roughly as $\partial M/\partial m_U \sim m_U \phi(m_U) \propto m_U^{-1.35}$ and $\partial L/\partial m_U \sim m_U^2 \phi(m_U) \propto m_U^{-0.35}$, respectively.

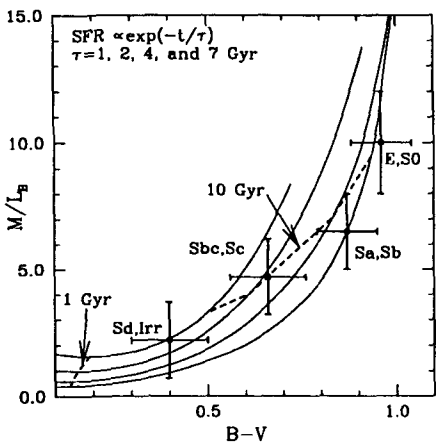

Fig. 9. Mass-to-blue light ratio versus $B-V$ color for the same models as in Fig. 7, compared to the values observed in nearby galaxies of various morphological types.

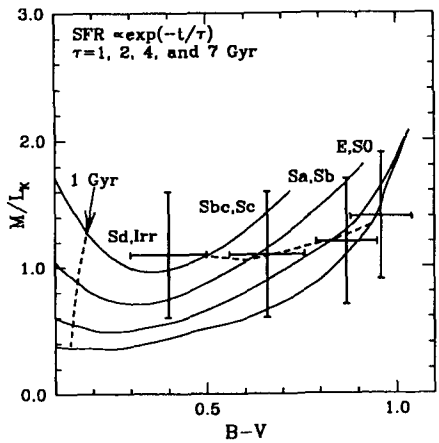

Fig. 10. Mass-to-infrared light ratio versus $B-V$ color for the same models as in Fig. 7, compared to the values observed in nearby galaxies of various morphological types.

Figures 9 and 10 show M/L_B and M/L_K as a function of $B-V$ color for models with the same range of star formation histories as in Figure 7. Traditionally, such ratios are expressed in units of $M_\odot/L_\odot$, where $L_\odot$ stands for the solar luminosity in the band under consideration (i.e., $L_{\odot B}$ and $L_{\odot K}$ in Figs. 9 and 10, respectively). As expected from Figure 7, the mass-to-blue light ratio increases with increasing color because, as a stellar population ages, the optical luminosity declines and the colors redden. However, Figure 10 shows that the mass-to-infrared light ratio is almost insensitive to the star formation history (note that the vertical scale is 5 times smaller in Fig. 10 than in Fig. 9). This is all the more remarkable in that different types of stars dominate the infrared light at different ages in an evolving stellar population (supergiants, AGB, and RGB stars; see Fig. 8). This interesting property renders mass estimates from the infrared light of galaxies more reliable than estimates from the optical light, although the infrared light does not traces only old (RGB) stars, as is often assumed. We also note that, again, models with timescales of star formation ranging from 1 to 7 Gyr are found to reproduce the mass-to-light ratios ob-

served in nearby galaxies of early to late morphological types, respectively. One of the reasons for this success is that observations refer to the mass within the Holmberg radii of the galaxies, i.e., where the photographic (essentially V) surface brightness reaches 26.5 mag arcsec^{-2}. Within this radius, the contribution to the mass by dark matter halos is not expected to be larger than 25% (Ostriker & Caldwell).

1.3 Uncertainties in the Modeling of Stellar Populations

The use of population synthesis models to recover the mixture of stars in a galaxy from observations of the integrated light suffers from various uncertainties. As we have seen above, part of the problem is that spectral evolution depends essentially only on the ratio of the present to past-averaged star formation rates. Another problem is that both age and metallicity have a similar effect on integrated colors and line strengths. As emphasized by Worthey (1994), if two stellar populations differ in age and metallicity by $d\log \mathrm{age}/d\log Z \approx 3/2$, they will appear virtually identical in all colors and most optical spectral indices (such as the characteristic absorption lines of prominent atoms and molecules). To illustrate this, we show in Figure 11 the evolution of the $B-V$ and $V-K$ colors and M/L_V mass-to-light ratio for instantaneous-burst stellar populations with fixed IMF and different metallicities. The main effect of increasing metallicity is to redden the colors and increase M/L_V at fixed age, which is similar to the effect of increasing age at fixed metallicity. The reason for this is that, at higher metallicity, stellar effective temperatures and luminosities are lower (see, e.g., Schaller et al. 1992; Fagotto et al. 1994).

Unfortunately, this "age-metallicity degeneracy" is further aggravated by significant differences among existing models in the predicted spectral properties of a stellar population with fixed age and metallicity. These discrepancies are caused by uncertainties in the main underlying assumptions of population synthesis models: the stellar evolution theory used to predict the distribution of stars in the theoretical H-R diagram and the library of spectra assigned to stars as a function of temperature, luminosity, and metallicity from which colors are calculated. Figure 12 shows the $B-V$ and $V-K$ colors and M/L_V ratio predicted for an instantaneous burst stellar population with solar metallicity and fixed IMF according to several recent population synthesis models (Bruzual & Charlot 1996 using the Geneva [B&C] and Padua [B&C alt.] tracks; Bertelli et al. 1994 [BBCFN]; Worthey 1994 [GW]). The deviations of 0.05 mag in $B-V$ color, 0.25 mag in $V-K$ color, and 25% in M/L_V are large compared to typical observational uncertainties, and they imply alarming ambiguities in the interpretation of galaxy colors. Charlot, Worthey, & Bressan (1996) have investigated in detail the sources of disprepancies in the predictions of current population synthesis models. They conclude that the main source of disagreement is the stellar evolution theory that relies on several critical factors which are either not sufficiently understood or cannot yet be determined uniquely from comparisons with observations (opacities, heavy element mixture, helium content, convection, diffusion, mass loss, rotational mixing). Differences in spectral calibrations

appear to have smaller consequences, although some major limitations are the difficult spectral modeling of cool stars and the unavailability of calibration stars for metal-rich populations and populations with altered chemical mixes.

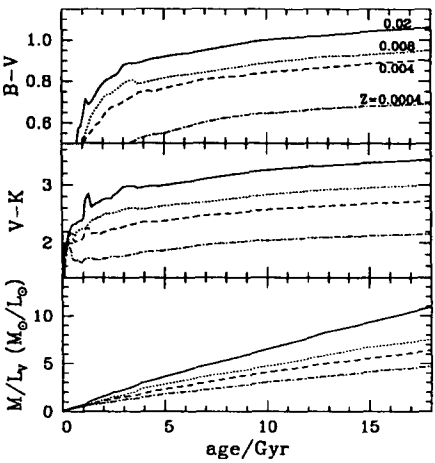

Fig. 11. Evolution of the $B-V$ and $V-K$ colors and M/L_V ratio for instantaneous burst stellar populations with different metallicities and a Salpeter IMF. Increasing metallicity reddens the colors and lowers the luminosity at fixed age.

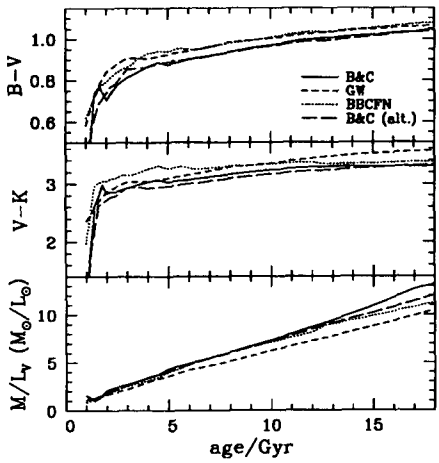

Fig. 12. Evolution of $B-V$, $V-K$, and M/L_V for an instantaneous burst stellar population with solar metallicity and a Salpeter IMF, according to various recent population synthesis models (see text for sources).

It is worth noting that the significant differences in the predictions of the various models in Figure 12 cannot be straightforwardly resolved by means of comparisons with observations. In fact, the models all compare to the observed colors of star clusters and galaxies approximately in a similar way. This is shown in Figure 13, in which the $B-V$, $U-V$, and $V-K$ colors of the solar-metallicity models of Figure 12 are plotted for ages 1 to 18 Gyr against integrated colors for Galactic and M 31 globular clusters (Burstein et al. 1984), LMC clusters older than about 1 Gyr (van den Bergh 1981; Persson et al. 1983), and elliptical and S0 galaxies (Frogel et al. 1978; Peletier 1989). The general agreement between model and observed color sequences is all the more remarkable in that the data, unlike the models, include a wide range of metallicities. Globular clusters have metallicities in the range $0.0001 \lesssim Z \lesssim 0.006$ and are presumably uniformly old (e.g. Hesser 1993). Elliptical and S0 galaxies probably contain several generations of stars (see also §2.4 below), although they usually are not expected to have experienced large recent bursts of star formation. According to González (1993), the dominant stellar populations in these galaxies would have metallicities slightly less than twice solar. The younger LMC clusters in Figure 2 (with ages $\gtrsim 1$ Gyr) have $Z \approx 0.01$, but the older clusters are probably as metal-poor as Galactic globular clusters (e.g., Cohen 1982).

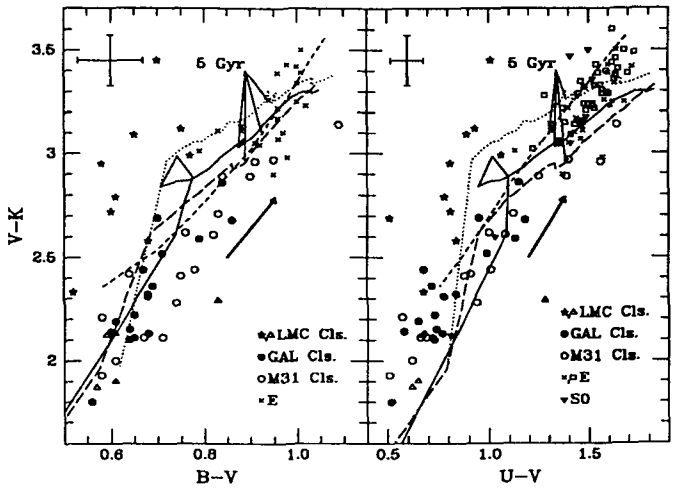

Fig. 13. Comparison of the $B-V$, $U-V$, and $V-K$ colors predicted by the solar-metallicity models of Fig. 12 at ages 1 to 18 Gyr with observed colors for star clusters and galaxies (all corrected for reddening). Model loci at 5 Gyr are also marked. The observations include Galactic and M 31 globular clusters (Burstein et al. 1984), LMC clusters (van den Bergh 1981; Persson et al. 1983), and nearby elliptical and S0 galaxies (*crosses*: Peletier 1989; *squares* and *upside down triangles*: Frogel et al. 1978). The LMC clusters are divided into two categories: upright triangles refer to the oldest clusters (type VII in the Searle, Wilkinson, & Bagnuolo 1980 classification), and stars refer to younger clusters (types IV, V, and VI). Conservative maximum observational error bars are indicated on the top left of each panel. Arrows representing the effect of reddening for $E(B-V)=0.1$ mag indicate how extinction can further aggravate the age-metallicity degeneracy.

Figure 13 illustrates the lack of clear diagnostic diagrams in integrated broad-band colors for population synthesis models. For example, while at fixed metallicity colors tend to redden with age (Fig. 5), the higher metallicity of the younger LMC clusters in Figure 13 causes their colors to be redder than those of the old, more metal-poor clusters. We note that the scatter in $V-K$ color for the younger LMC clusters is caused by the high sensitivity of the integrated light to the presence of even a few extremely cool TP-AGB carbon stars in these objects. Furthermore, the relatively blue colors in Figure 13 of one S0 galaxy of nearly solar metallicity which recently underwent a burst of star formation (the local group galaxy NGC 205 with $V-K=2.1$ and $U-V=0.8$; e.g., Davidge 1992) coincide with the colors of the most metal-poor, oldest clusters in the Galaxy. This provides dramatic empirical evidence of the severity of the age-metallicity degeneracy. Also, the overall match by solar-metallicity models to the color sequences of star clusters and early-type galaxies is another example

of this degeneracy. Extinction can further aggravate the age-metallicity degeneracy, as reddening vectors are parallel to the age/metallicity color sequences in Figure 13.

The main interest in population synthesis models is generally the determination of age, metallicity, and mass of galaxies from their observed spectral energy distributions. The uncertainties associated to such determinations can be estimated from the dispersion in the predictions of current population synthesis models relying on different input stellar models and spectra. Such an analysis indicates that, for idealized galaxies containing a single generation of stars and no dust, properties derived from broad-band colors and most optical spectral indices are accurate by roughly $\pm 35\%$ in age at fixed metallicity, 25% in metallicity at fixed age if the heavy element mixture is assumed to be scaled-solar, and 35% in mass at fixed metallicity and fixed IMF (Charlot et al. 1996). Even for idealized galaxies defined in this way, the uncertainties in age and metallicity determinations will increase, as expressed by the age-metallicity degeneracy, if both quantities are allowed to vary. For real galaxies containing several generations of stars with different metallicities (and perhaps even dust), determinations of age, metallicity, and mass of the various components will be far more uncertain. Finally, we note that in the gas-rich environments of star forming galaxies, nebular emission by recombination of hydrogen, helium, and heavy elements ionized by young stars is another major source of uncertainties as it can contribute significantly to the integrated light (Charlot 1996; García-Vargas, Bressan, & Leitherer 1996).

2 The Appearance of Galaxies at High Redshifts

2.1 Introduction

The expected widespread population of high-redshift analogs or progenitors of present-day disk galaxies has still not been observed in emission. This leaves large uncertainties on the appearance of young galaxies (see White 1989; Pritchet 1994). Early models predicted that "primeval galaxies" undergoing strong starbursts at redshifts $z \gtrsim 2$ should be detectable at magnitudes $R \sim 21 - 23$, but deep spectroscopic surveys to $B \lesssim 22.5$, $I \lesssim 22.1$, and $K \lesssim 20$ have not revealed such a population of forming galaxies (Partridge & Peebles 1967; Meier 1976; Colless et al. 1993; Cowie et al. 1994; Lilly et al. 1995). Partridge and Peebles (1967) pointed out that Lyα emission could be the most prominent and easily detectable signature of primeval galaxies. The reason for this is that the ionizing radiation from young stars in galaxies should lead to a strong and narrow Lyα line by recombination of the hydrogen in the ambient interstellar medium, which would be more readily visible than continuum radiation against the sky noise. A few galaxy-like objects have been discovered at redshifts $z \lesssim 4$, which occasionally show strong Lyα emission (Pritchet 1994; Spinrad 1989; Macchetto et al. 1993; Rowan-Robinson et al. 1993). However, most of these objects are peculiar, and their connection to present-day galaxies is not at all clear. In fact, all blank sky searches for Lyα emission from ordinary galactic disks at high redshifts have

given null results, suggesting that young galaxies form stars slowly or in large volumes, or that Lyα photons are absorbed by dust (see Baron & White 1987, and references therein).

Independently, much has been learned on the distribution of HI in the universe at redshifts $z \lesssim 3.5$ from absorption-line studies of distant quasars (see for example Petitjean et al. 1993). The strongest absorption lines are attributed to the damped Lyα systems, that are generally interpreted as the best candidates for ordinary galactic disks at high redshift (Lanzetta et al. 1991). These have observed HI column densities $N_{\rm HI} \gtrsim 2 \times 10^{20}\,{\rm cm}^{-2}$, and their abundances in heavy elements and dust at $z \approx 2.5$ amount to about 10% of the values in the Milky Way (Pei et al. 1991; Pettini et al. 1994). The damped Lyα systems do not show Lyα emission at the level expected from young, dust-poor disk galaxies (see Pettini et al. 1994). Alternatively, the evolution with redshift of the gas density integrated over all HI absorbers, $\Omega_{\rm HI}(z)$, provides some constraint on the global depletion of cold gas though star formation in the universe since $z \approx 3.5$ (Lanzetta et al. 1995; Pei & Fall 1995). Absorption-line systems of distant quasars have also been used successfully as a way to select normal galaxies in emission out to $z \approx 1.6$ against the population of relatively nearby blue galaxies that dominate galaxy number counts at faint magnitudes (Bergeron 1988; Steidel & Dickinson 1995; Steidel et al. 1995; Aragón-Salamanca et al. 1994). These studies have shown that field galaxies with luminosities around L^* exhibit only little evolution in their space density, luminosity, and optical/infrared colors at redshifts $0.2 \lesssim z \lesssim 1.6$.

Recent observations therefore seem to indicate that the formation and evolution of normal disk galaxies has been less spectacular than originally thought. In what follows, we explain how the apparent lack of Lyα emission from young galaxies at high redshift is probably mainly a consequence of the relatively brief periods in which primeval galaxies are dust-free, and hence Lyα-bright. In fact, most present observational constraints on young galaxies appear to be in agreement with the predictions of theories based on hierarchical clustering, in which galaxies form slowly and relatively recently. The very blue, primeval galaxy phase expected at the onset of star formation would then be faint and short-lived. Since at redshifts $z \gtrsim 2$ galaxies are expected to be difficult to detect, one may think of using population synthesis models to trace back the early history of star formation from observations at lower redshifts. We also discuss below the limitations of this approach.

2.2 Lyman-Alpha Emission from Young Galaxies

The observed Lyα emission from a young galaxy depends on the star formation rate and IMF, but also on several other factors: the contributions by supernova remnants and active galactic nuclei, the orientation of the galaxy, and absorption by dust. The contribution to the Lyα emission by stars can be estimated using stellar population synthesis models. We assume for the moment that circumstellar HII regions are the only sources of Lyα photons and that the column density of the ambient HI is large enough that case B recombination applies

($N_{\rm HI} \gtrsim 10^{17}\,{\rm cm}^{-2}$) but otherwise ignore the effects on the interstellar medium on the transfer of Lyα photons. Under these "minimal" assumptions and using recent population synthesis models, Charlot & Fall (1993) have shown that the Lyα emission from a galaxy depends sensitively on the age and IMF slope, even when the star formation rate is constant. The dependence on the IMF upper cutoff and metallicity, on the other hand, are much weaker. Thus, only a rough estimate of the Lyα equivalent width of a young, dust-free galaxy is permitted, about $50 - 120$ Å.

We now briefly review the other factors that can affect the observed Lyα emission from a young galaxy (see Charlot & Fall 1993 for more details). Shull & Silk (1979) have computed the time-averaged, Lyα luminosity of a population of Type II supernova remnants using a radiative-shock code with low metallicity. Their results indicate that the contribution to the Lyα emission by supernova remnants is always less than the contribution by stars (typically 10% for a solar-neighborhood IMF) and can therefore be neglected. Active Galactic Nuclei (AGNs) are another potential source of ionizing radiation in a galaxy. We assume for simplicity that the spectrum of an AGN can be approximated by a power law $f_\nu \propto \nu^{-\alpha}$ with an index blueward of Lyα in the range $1 \lesssim \alpha \lesssim 2$. If we also assume that the AGN is completely surrounded by HI, that case B recombination applies, and that absorption by dust is negligible, then the Lyα equivalent width is $827\alpha^{-1}(3/4)^\alpha$ Å, or 600 Å for $\alpha = 1$ and 200 Å for $\alpha = 2$. The fact that most bright quasars have observed Lyα equivalent widths in the range $50-150$ Å could reflect a partial covering of the AGNs by HI clouds in the broad-line regions (in fact, some ionizing radiation escapes from quasars), attenuation of the Lyα emission by dust, or orientation effects (see below). Thus, in principle, AGNs can produce higher Lyα equivalent widths than stellar populations. However, the presence of an AGN in a galaxy is usually revealed by other readily identifiable signatures: strong emission lines of highly ionized species (CIV, HeII, etc.) and broad emission lines with velocity widths several times larger than those expected from the virial motions within galaxies.

The Lyα photons produced in galaxies will suffer a large number of resonant scatterings in the ambient neutral atomic hydrogen. In the absence of dust, this would lead to no net enhancement of the angle-averaged Lyα emission from a galaxy or of the total Lyα emission from a sample of randomly-oriented galaxies. However, since the Lyα line is emitted more isotropically than the continuum, the Lyα equivalent width of an individual galaxy will decrease as it is viewed more nearly edge-on. For example, in the idealized case of a plane-parallel slab, the ratio of the observed to angle-averaged Lyα equivalent width will decrease from 2.3 to 0 for viewing angles to the normal ranging from 0° to 90°. The resonant scattering of Lyα photons by HI also increases enormously their chances of absorption by dust grains. The attenuation is expected to be important when the dimensionless dust-to-gas ratio, defined in terms of the extinction optical depth in the B band by $k \equiv 10^{21}(\tau_B/N_{\rm HI})\,{\rm cm}^{-2}$, exceeds the critical value $k_{\rm crit} \approx 0.01(N_{\rm HI\perp}/10^{21}\,{\rm cm}^{-2})^{-4/3}(\sigma_V/10\,{\rm km\,s}^{-1})^{2/3}$ (see Charlot & Fall 1993). In this expression, $N_{\rm HI\perp}$ and σ_V are the face-on column density and line-of-sight

velocity dispersion of HI. For reference, the dust-to-gas ratio in the Milky Way and Large and Small Magellanic Clouds are, respectively, $k \approx 0.8$, $k \approx 0.2$, and $k \approx 0.02$, and the face-on HI column densities within the optically visible regions of most spiral galaxies lie in the range $10^{20} \lesssim N_{\rm HI\perp} \lesssim 10^{21}\,{\rm cm}^{-2}$. Thus, we expect $k \gtrsim k_{\rm crit}$ unless the dust-to-gas ratio is much smaller than the value in the Milky Way. In particular, some attenuation of the Lyα emission by dust is expected in the damped Lyα systems, since $N_{\rm HI} \gtrsim 2 \times 10^{20}\,{\rm cm}^{-2}$ and $k \approx 0.1$ (although there may be a large dispersion around this value; see Pei et al. 1991; Pettini et al. 1994). Moreover, the attenuation of Lyα emission by dust depends sensitively on the structure of the interstellar medium in a galaxy. In the case of a multiphase medium, the transfer of Lyα photons will depend largely on the topology of the interfaces between HI and HII regions (see Spitzer 1978; Neufeld 1991). As a result of these complications, it is nearly impossible to deduce star formation rates from the observed Lyα emission of a galaxy.

The above arguments may be used to interpret the observations of and searches for Lyα emission from nearby star-forming galaxies, damped Lyα systems, blank sky, and the companions of quasars and damped Lyα systems (see Charlot & Fall 1993). It appears that, when Lyα emission is weak or absent, as is the case in most star-forming galaxies at low redshifts and in damped Lyα systems at high redshifts, the observed abundance of dust is sufficient to absorb most of the Lyα photons. On the other hand, when Lyα emission is strong, the presence of highly ionized species, large velocity widths, or nearby quasars indicate that much of the ionizing radiation may be supplied by AGNs. The hope has always been that the searches for Lyα emission at high redshifts would reveal a population of primeval galaxies, in which the abundances of heavy elements and hence dust were low enough that most of the Lyα photons could escape. Such a population may exist at some redshifts. However, since the Lyα emission is attenuated when the dust-to-gas ratio exceeds $1 - 10\%$ of the value in the Milky Way, a typical galaxy probably spends only the first few percent of its lifetime in a Lyα-bright phase. We therefore expect primeval galaxies, as defined above, to be relatively rare at most redshifts, consistent with the null results of all searches to date.

2.3 What Should Young Galaxies Look Like?

If galaxies undergoing their first episodes of star formation in the young universe resemble nearby examples of starburst galaxies, one would expect them to exhibit very blue continua and strong Balmer emission lines. However, the most distant counterparts of nearby disk galaxies found by association with quasar absorption-line systems do not show such extreme signatures (Steidel & Dickinson 1995; Aragón-Salamanca et al. 1994). Instead, out to $z \approx 1.6$, normal field galaxies appear to display strikingly little evolution in their space density, luminosity, and optical/infrared colors (most of the evolution appears to be confined in the faint end of the galaxy luminosity function). Other constraints on the history of star formation in galaxies, and hence on their appearance, may be obtained from the evolution of the integrated neutral gas density of the universe. Recent surveys

indicate that the total amount of gas in damped Lyα systems at a redshift $z \approx 3.5$ could be nearly as high as the total density of luminous material in present-day galactic disks (Lanzetta et al. 1995; Wolfe 1995). This would imply that most stars have formed relatively recently, consistent with the expectation from theories of galaxy formation based on hierarchical clustering (although a precise interpretation of the observed $\Omega_{\rm HI}$ evolution requires including the effect of quasar obscuration by dust in damped Lyα systems; see Pei & Fall 1995).

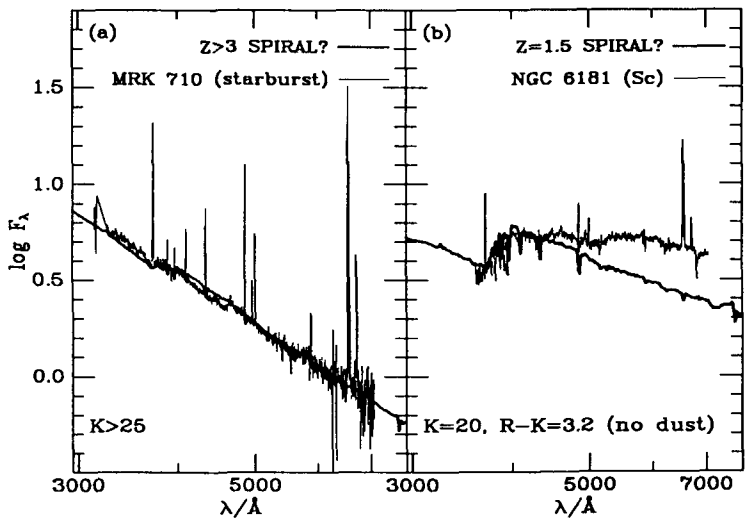

Fig. 14. (a) Possible appearance of a progenitor spiral galaxy at $z > 3$ satisfying the current observational constraints on the evolution of $\Omega_{\rm HI}(z)$ and the observed properties of the Milky Way in a standard cold dark matter universe (thick line) compared to the observed spectrum of the nearby starburst galaxy Mrk 710 (thin line). The model spectrum does not include emission lines (see text for more details). (b) Same model galaxy as in (a) viewed at $z = 1.5$ and compared to the observed spectrum of the nearby spiral galaxy NGC 6181. The spectra in (a) and (b) are in the rest frames of the galaxies, and the predicted apparent K magnitudes (and $R - K$ color at $z = 1.5$) are indicated at the bottom.

A natural question to ask, then, is what do models accommodating present observational constraints predict for the appearance of very young galaxies? To answer this question, we have computed the early spectral evolution of a spiral galaxy using a combination of the Kauffmann et al. (1993) semi-analytic model of galaxy formation and the Bruzual & Charlot (1993) population synthesis code. The star formation rate can be adjusted to reproduce both the evolution of $\Omega_{\rm HI}(z)$ at $z \lesssim 3.5$ in a standard cold dark matter universe and the spectral energy distribution of a typical nearby spiral galaxy at $z = 0$ (see Kauffmann & Charlot

1994). The early spectral evolution of this model is presented in Figure 14. Figure 14a shows that the galaxy undergoes an extremely blue phase at $z > 3$, during which the spectrum resembles the observed spectrum of the nearby starburst galaxy Mrk 710 with strong H-Balmer and oxygen emission lines (from Vacca & Conti 1992). At this time, the young galaxy could qualify as a "primeval galaxy" as defined earlier. However, the phase is short-lived ($\lesssim 10^7$ yr) and very faint ($K > 25$). Then, the onset of evolved supergiant, asymptotic giant branch, and red giant branch stars reddens the spectrum substantially. At $z = 1.5$, twenty percent of the stars present at $z = 0$ have formed, and the model galaxy in Figure 14b has $K \approx 20$ and $R - K \approx 3.2$, i.e., a spectrum only moderately bluer than that of the nearby spiral galaxy NGC 6181 (from Kennicutt 1992). These predicted colors, which ignore reddening by dust, are interestingly close to the observed $K \approx 19.5$ and $R - K \approx 4$ of galaxies discovered at $z \approx 1.5$ in association with quasar absorption-line systems (Steidel & Dickinson 1995). Hence, the present results would reinforce the suggestion that the spectra of normal disk galaxies have evolved only moderately for much of their lifetime. The extremely blue phase at the onset of star formation, which might coincide with a Lyα-bright phase, is expected to be, on average, much fainter and short-lived (this initial phase may be brighter for elliptical galaxies if these formed most of their stars in an initial strong burst of star formation).

2.4 Tracing Back the History of Star Formation in Galaxies

Since young galaxies may be hard to detect at redshifts beyond $z \sim 2$, an alternative is to try and trace back the earlier history of star formation from observations at lower redshifts. The conventional approach to this problem is to use stellar population synthesis models and search for the evolution of the star formation rate that will reproduce the observed spectral characteristics of galaxies. As we have seen in §1, the degeneracy of galaxy spectra in age, metallicity, and history of star formation hampers the dating of passively evolving stellar populations such as elliptical galaxies from the single knowledge of the continuum spectrum, or equivalently, of broad-band colors. Furthermore, from the continuum spectra of spiral galaxies, one can at best obtain ratios of present to past-averaged star formation rates.

Some additional information on the past history of star formation in galaxies may be learned from the stellar absorption lines of hydrogen and of other prominent atoms and molecules (such as Mg, Mg_2, Fe, Ca, Na, Sr, and CN), even though most optical spectral indices appear to be degenerate in age and metallicity. For example, main-sequence A and B stars (that have lifetimes $\lesssim 2$ Gyr) are expected to strengthen the H-Balmer series and weaken the prominent metallic lines in the integrated galaxy spectrum. This can be most simply illustrated by considering the case of intermediate-age stellar populations in early-type galaxies. There is growing photometric and dynamical evidence that many E/S0 galaxies have formed stars only a few billion years ago (Pickles 1989; Rose 1985; Schweizer & Seitzer 1992; and references therein). The prototypical example is

the dwarf elliptical galaxy M 32, which is believed to have undergone substantial star formation until only about 5 Gyr ago (e.g., O'Connell 1980).

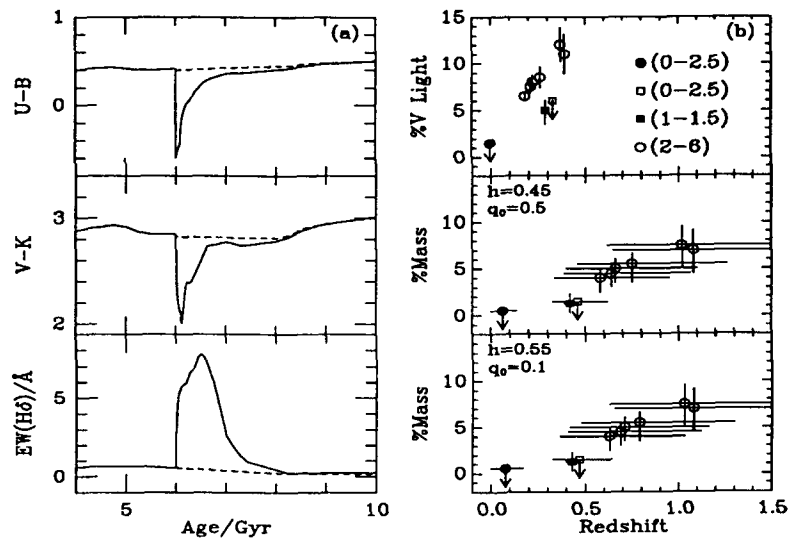

Fig. 15. (a) Evolution of the $U - B$ and $V - K$ colors and Hδ absorption equivalent width of a model elliptical galaxy formed in a single burst at $t = 0$ (dashed line) and of a similar model galaxy on which a new burst involving 10% of the final mass is added at an age of 6 Gyr (solid line). (b) Upper panel: observed contributions by intermediate-age stars to the V luminosity of E/S0 galaxies at $z \approx 0$ and in low-redshift clusters inferred from stellar absorption-line studies (see text for sources). Different symbols correspond to different studies or different ranges of intermediate ages (indicated in Gyr). Lower panels: mass fraction of stars formed in the progenitors of E/S0 galaxies as a function of redshift derived for two cosmologies from the observations shown in the upper panel. The horizontal error bars follow from the uncertainties on the ages of stars detected in low-redshifts E/S0 galaxies. The vertical error bars follow from the uncertainties on the determination of the contribution by these stars to the mass for the allowed range of ages.

Figure 15a illustrates how spectral absorption features such as the Balmer Hδ equivalent width can be used to detect late bursts of star formation in early-type galaxies with colors otherwise typical of old, passively evolving stellar populations. The solid lines correspond to a model elliptical galaxy formed in a major burst at age $t = 0$, on which a new burst involving 10% of the final mass is added at an age of 6 Gyr. At ages $t > 6.5$ Gyr, the $U - B$ and $V - K$ colors of this model differ by less than 0.1 mag from the values in the absence a second burst (shown by the dashed lines). However, the Hδ equivalent width continues to evolve significantly for nearly 1 Gyr because of the presence of A and B stars.

Pickles (1989) and Rose (1985) have shown, using other stellar absorption lines, how similar diagnostics can be used to discriminate between different generations of stars in E/S0 galaxies and, to some extent, to untangle the competing effects of age and metallicity on the spectra. Worthey (1994) has also recently produced a comprehensive study of the absorption-line characteristics of old stellar populations and their dependence on age and metallicity.

We now briefly exemplify some implications of these arguments for the history of star formation in early-type galaxies (see Charlot & Silk 1994 for more details). In the upper panel of Figure 15b we have compiled estimates of the typical fraction of optical light accounted for by intermediate-age stars in normal E/S0 galaxies at redshifts $z \lesssim 0.4$ from several studies of stellar absorption-lines strengths (Rose 1985; Pickles 1989; Couch & Sharples 1987). At $z \gtrsim 0.1$, most galaxies were selected in clusters (the estimates are based on all red galaxies with luminosities $\lesssim L^*$ for which spectra were available at each redshift). In each case, the range of intermediate ages attributed to the stars is indicated in billion years. In the lower two panels of Figure 15b, we have reexpressed these constraints on the ages of stellar populations into constraints on the redshifts of formation for two cosmologies using the Bruzual & Charlot (1993) population synthesis models. A flat universe with $q_0 = 0.5$ and $h = 0.45$, and an open universe with $q_0 = 0.1$ and $h = 0.55$ (where $h = H_0/100\,\mathrm{km\,s^{-1}Mpc^{-1}}$). Both correspond to a present age of the universe of about 15 Gyr and lead to similar predictions: the mass fraction of stars formed in E/S0 galaxies has decreased smoothly with time, from about 8% at $z \approx 1$ to less than 1% at $z \approx 0$ (see also Pickles 1989; Schweizer & Seitzer 1992). This evolution of the star formation rate inferred from stellar absorption-line studies is in reality a mean evolution averaged over large redshift intervals, as the horizontal error bars indicate. It does not imply that E/S0 galaxies should form stars at all times. In fact, the ages of intermediate-age stars estimated from absorption-line strengths in the spectra of galaxies at low redshifts are uncertain by a few billion years. As Figure 15a shows, after a galaxy undergoes a burst of star formation, the colors reach the values characteristic of old, passively evolving stellar populations in less than 1 Gyr. Thus, although galaxies at low redshift may present similar signatures of past star formation, there should be a dispersion in the ages and hence colors of the progenitor galaxies at high redshift around the value corresponding to the mean epoch of star formation estimated in the lower panels of Figure 15b. The relevance of this result for the evolution of galaxies in clusters has been investigated by Charlot & Silk (1994; see also Belloni et al. 1995).

Unfortunately, stellar absorption-line strengths cannot yet be used to trace back the history of star formation in spiral galaxies. The reason for this is that the best-known stellar absorption features arise at ultraviolet and optical wavelengths, where the spectral signatures of old and intermediate-age stars in spiral galaxies are hidden by the strong continuum light of young massive stars. The situation may soon be improved, as substantial progress is underway to understand the infrared spectral signatures of old stars in star-forming galaxies (Lançon &

Rocca-Volmerange 1995). However, tracing back the onset of star formation in normal disk galaxies still appears to be a long way ahead.

References

Arimoto, N., Yoshii, Y. (1987), A&A, Vol. 173, p. 23.

Aragón-Salamanca, A., Ellis, R.S., Schwartzenberg, J.M., Bergeron, J. (1994), ApJ, Vol. 421, p. 27.

Baron, E., White, S.D.M. (1987), ApJ, Vol. 322, p. 585.

Belloni, P., Bruzual A., G., Thimm, G.J., Rose, H.J. (1995), A&A, Vol. 297, p. 61.

Bergeron, J. (1988), in *Large Scale Structures in the Universe*, Int. Astron. Union Symp. No. 130 (Reidel), p. 343.

Bressan, A., Fagotto, F., Bertelli, G., Chiosi, C. (1993), A&AS, Vol. 100, p. 647.

Bressan, A., Chiosi, C., Fagotto, F. (1994), ApJS, Vol. 94, p. 63.

Bruzual A., G. (1983), ApJ, Vol. 273, p. 105.

Bruzual A., G., Charlot, S. (1993), ApJ, Vol. 405, p. 538.

Bruzual A., G., Charlot, S. (1996), ApJ, in preparation.

Burstein, D., Faber, S.M., Gaskell, C.M., Krumm, N. (1984), ApJ, Vol. 287, p. 586.

Buzzoni, A. (1989), ApJS, Vol. 71, Vol. 817.

Caldwell, J.A.R., Ostriker, J.P. (1981), ApJ, Vol. 251, p. 61.

Charlot, S. (1996), in *From Stars to Galaxies*, ed. C. Leitherer, U. Fritze-van Alvensleben, & J. Huchra (ASP Conference Series), in press.

Charlot, S., Bruzual A., G. (1991), ApJ, Vol. 367, p. 126.

Charlot, S., Fall, S.M. (1993), ApJ, Vol. 415, p. 580.

Charlot, S., Silk, J. (1994), ApJ, Vol. 432, p. 453.

Charlot, A., Worthey, G., Bressan, A. (1996), ApJ, Vol. 457, in press.

Cohen, J.G. (1982), ApJ, Vol. 258, p. 143.

Colless, M., Ellis, R.S., Broadhurst, T.J., Taylor, K., Peterson, B.A. (1993), MNRAS, Vol. 261, p. 19.

Couch, W.J., Sharples, R.M. (1987), MNRAS, Vol. 229, p. 423.

Cowie, L.L., Gardner, J.P., Hu, E.M., Songaila, A., Hodapp, K.-W., Wainscoat, R.J. (1994), ApJ, Vol. 434, p. 114.

Crampin, J., Hoyle, F. (1961), MNRAS, Vol. 122, p. 27.

Davidge, T.J. (1992), ApJ, Vol. 397, p. 457.

Fagotto, F., Bressan, A., Bertelli, G., Chiosi, C. (1994), A&AS, Vol. 100, p. 647.

Fritze von Alvensleben, U.A., Gerhard, O.E. (1994), A&A, Vol. 285, p. 751.

Frogel, J.A., Persson, S.E., Aaronson, M., Mathews, K. (1978), ApJ, Vol. 220, p. 75.

Gallagher, J.S., Hunter, D.A., Tutukov, A.V. 1984, ApJ, Vol. 284, p. 544.

García-Vargas, M.L., Bressan, A., Leitherer, C. (1996), in preparation.

González, J.J. (1993), Ph.D. Thesis, Univ. of California, Santa Cruz.

Guiderdoni, B., Rocca-Volmerange, B. (1987), A&A, Vol. 186, p. 1.

Hesser, J.E. (1993), in *The Globular Cluster-Galaxy Connection*, ed. Smith & Brodie (ASP Conference Series, Vol. 48), p. 1.

Kauffmann, G., Charlot, S. (1994), ApJ, Vol. 430, p. L97.

Kauffmann, G., White, S.D.M., Guiderdoni, B. (1993), MNRAS, Vol. 274, p. 201.

Kennicutt, R.C. (1992), ApJS, Vol. 79, p. 255.

Kennicutt, R.C., Tamblyn, P., Congdon, C.W. (1994), ApJ, Vol. 435, p. 22.

Lançon, A., Rocca-Volmerange, B. (1995), A&A, preprint.

Lanzetta, K.M., Wolfe, A.M., Turnshek, D.A., Lu, L.M., McMahon, R.C., Hazard, C. (1991), ApJS, Vol. 77, p. 1.
Lanzetta, K.M., Wolfe, A.M., Turnshek, D.A. (1995), ApJ, Vol. 440, p. 435.
Larson, R.B. (1986), MNRAS, Vol. 218, p. 409.
Lilly, S.J., Tresse, L., Hammer, F., Crampton, D., Le Fevre, O. (1995), ApJ, preprint.
Macchetto, F., Lipari, S., Giavalisco, M., Turnshek, D.A., Sparks, W.B. (1993), ApJ, Vol. 404, p. 511.
Mayya, Y.D. (1995), AJ, Vol. 109, p. 2503.
Meier, D. (1976), ApJ, Vol. 207, p. 343.
Neufeld, D.A. (1991), ApJ, Vol. 370, p. L85.
O'Connell, R.W. (1980), ApJ, Vol. 236, p. 430.
Oke, J.B., Gunn, J.E. (1983), ApJ, Vol. 266, p. 713.
Partridge, R.B., Peebles, P.J.E. (1967), ApJ, Vol. 147, p. 868.
Pei, Y.C., Fall, S.M., Bechtold, J. (1991), ApJ, Vol. 378, p. 6.
Pei, Y.C., Fall, S.M. (1995), ApJ, in press.
Peletier, R.F. (1989), Ph.D. thesis, Univ. of Groningen.
Persson, S.E., Aaronson, M., Cohen, J.G., Frogel, J.A., Mathews, K. (1983), ApJ, Vol. 266, p. 105.
Petitjean, P., Webb, J.K., Rauch, M., Carswell, R.F., Lanzetta, K.M. (1993),
Pettini, M., Smith, L.J., Hunstead, R.W., King, D.L. (1994), ApJ, Vol. 426, p. 79.
Pickles, A.J. (1989), in *The Epoch of Galaxy Formation*, ed. C.S. Frenk, R.S. Ellis, T. Shanks, A.F. Heavens, J.A. Peacock (Kluwer), p. 191.
Rose, J. (1985), AJ, Vol. 90, p. 1927.
Rowan-Robinson, M., et al. (1993), MNRAS, Vol. 261, p. 513.
Salpeter, E.E. (1955), ApJ, Vol. 121, p. 161.
Scalo, J.M. (1986), Fundamentals of Cosmic Physics, Vol. 11, p. 1.
Schaller, G., Schaerer, D., Meynet, G., Maeder, A. (1992), A&AS, Vol. 96, p. 26.
Schweizer, F., Seitzer, P. (1992), AJ, Vol. 104, p. 1039.
Searle, L., Wilkinson, A., Bagnuolo, W.G. (1980), ApJ, Vol. 239, p. 803.
Shull, J.M., Silk, J. (1979), ApJ, Vol. 234, p. 427.
Silk, J. (1996), this volume.
Spinrad, H. (1989), in *The Epoch of Galaxy Formation*, ed. C.S. Frenk, R.S. Ellis, T. Shanks, A.F. Heavens, J.A. Peacock (Kluwer), p. 39.
Spitzer, L.: *Physical Processes in the Interstellar Medium* (Wiley)
Steidel, C.C., Dickinson, M. (1995), in *Wide Field Spectroscopy and the Distant Universe* (Cambridge University Press), in press.
Steidel, C.C., Dickinson, M., Persson, S.E. (1995), ApJ, Vol. 437., p. L75.
Thuan, T.X., Gunn, J.E. (1976), PASP, Vol. 88, p. 543.
Tinsley, B.M. (1978), ApJ, Vol. 222, p. 14.
Tinsley, B.M. (1980), Fundamentals of Cosmic Physics, Vol. 5, p. 287.
Vacca, W.D., Conti, P.S. (1992), ApJ, Vol. 401, p. 543.
van den Bergh, S. (1981), A&AS, Vol. 46, p. 79.
Weiss, A., Peletier, R.F., Matteucci, F. 1995, A&A, Vol. 296, p. 73.
White, S.D.M. (1989), in *The Interstellar Medium in Galaxies*, ed. H.A. Thronson & M. Shull (Kluwer), p. 371.
Wolfe, A.M. (1995), in *The Physics of the Interstellar Medium and Intergalactic Medium*, ed. A. Ferrara, C. Heiles, C. McKee, P. Shapiro (ASP Conference Series), in press
Worthey, G. (1994), ApJS, Vol. 95, p. 107.